

# On correlations of CM-type Maass waveforms under the horocyclic flow

Dennis A Hejhal<sup>1,2</sup> and Hans Christianson<sup>3</sup>

<sup>1</sup> Department of Mathematics, Box 480, Uppsala University, S-75106 Uppsala, Sweden

<sup>2</sup> School of Mathematics, University of Minnesota, Minneapolis, MN 55455, USA

<sup>3</sup> Department of Mathematics, University of California, Berkeley, CA 94720, USA

Received 30 July 2002

Published 12 March 2003

Online at [stacks.iop.org/JPhysA/36/3467](http://stacks.iop.org/JPhysA/36/3467)

## Abstract

Maass waveforms of CM-type are a special kind of eigenfunction of the hyperbolic Laplacian whose ‘defining’ components (namely eigenvalue and Fourier coefficients) are given by simple formulae involving algebraic integers chosen from a suitable number field  $K/\mathbb{Q}$ . In this paper, we report on some computer experiments aimed at ascertaining the extent to which the autocorrelation behaviour of CM-forms agrees with that of ‘mock’ (i.e. random) waveforms in the limit of high energy. Our results suggest that no significant differences are seen.

PACS number: 05.45.Mt

## 1. Background

Quantum chaos is a topic of natural interest on negatively curved Riemannian manifolds  $\mathcal{M}$ . This is a reflection of the well-known fact that the dynamics of a classical point particle traversing  $\mathcal{M}$  are typically ergodic (cf e.g. [10–12, 23] and the literature cited there). The simplest class of such manifolds is that associated with the set-up where  $\mathcal{M}$  is expressed as a quotient space  $\Gamma \backslash H$ ,  $\Gamma$  being a discrete subgroup of  $SL(2, \mathbb{R})$  and  $H$  the Poincaré upper half-plane  $\{\text{Im}(z) > 0\}$ . To ensure that  $\Gamma \backslash H$  has good geometry in the hyperbolic metric

$$ds^2 = \frac{dx^2 + dy^2}{y^2}$$

(the curvature here being  $-1$ ), one typically assumes that the hyperbolic area

$$\iint_{\Gamma \backslash H} \frac{dx dy}{y^2}$$

of  $\mathcal{M}$  is finite. From a dynamical perspective, a good portion of quantum chaos is then concerned with determining the extent to which high-frequency eigenfunctions of the hyperbolic Laplacian on  $\Gamma \backslash H$  simulate random waves as the frequency (or wave number) tends to infinity.

Maass waveforms  $\varphi$  are simply square-integrable eigenfunctions of the Laplacian on  $\Gamma \backslash H$ .

The standard framework for these from an *arithmetic* viewpoint is that where  $\Gamma$  is just  $SL(2, \mathbb{Z})$  or a finite-index subgroup thereof (more specifically, one of congruence type). Writing  $\lambda = \frac{1}{4} + R^2$  for the associated eigenvalue of  $-\Delta$ , the typical Maass waveform then admits a Fourier expansion of form

$$\varphi(x, y) = \sum_{n=1}^{\infty} c_n \sqrt{y} K_{iR}(2\pi ny) \begin{Bmatrix} \cos(2\pi nx) \\ \sin(2\pi nx) \end{Bmatrix}$$

wherein  $R > 0$  is tacitly assumed,  $K_{iR}(u)$  is the standard exponentially decaying  $K$ -Bessel function ([28]), and the  $c_n$  are appropriate real coefficients<sup>4</sup>. Matters are connected to wave mechanics by setting

$$\psi(x, y, t) = \varphi(x, y) e^{-iEt/\hbar}$$

and observing that

$$i\hbar \frac{\partial \psi}{\partial t} = -\frac{\hbar^2}{2m} \Delta \psi = -\frac{\hbar^2}{2m} y^2 (\psi_{xx} + \psi_{yy}) = E \psi$$

holds on  $H$  with  $\hbar = 1$ ,  $m = \frac{1}{2}$ ,  $E = \lambda = \frac{1}{4} + R^2$ . The number  $R^2$  can thus be regarded as a wave number.

Let  $\delta = \frac{\pi}{R}$ . In very rough terms,  $\varphi$  can be thought of as a standing ocean wave (in the hyperbolic geometry of  $\mathcal{M}$ ) having traditional wavelength  $(\text{const})\delta$  (cf [10, section 3]). The number  $2\delta (\sim 2\pi/\sqrt{E})$  is sometimes called the de Broglie wavelength.

The fact that  $\varphi$  ‘lives’ on  $\mathcal{M}$  simply means that  $\varphi$  is  $\Gamma$ -invariant (i.e. takes the same value at any two points of  $H$  equivalent under the action of  $\Gamma$ ). This hypothesis implies that only very special  $R$ -values and  $c_n$ ’s are possible on any given  $\Gamma$ .

The upshot of [10–12] is that value-distributionally on  $\mathcal{M}/(\text{the group of reflective symmetries})$ , the functions  $\varphi$  *do* appear to simulate random waves as  $R \rightarrow \infty$ , at least over robust two-dimensional subregions such as rectangles both of whose dimensions are kept bigger than about  $50\delta$  or so.

Following the seminal work of Berry [6], a host of papers have appeared dealing with various aspects of this ‘mimicry’ question in a multitude of more general geometric settings for  $\mathcal{M}$ ; cf [1, 4, 5, 18, 23] for a reasonable sampling.

One rather surprising aspect of the arithmetic setting is that, for certain very simple choices of  $\Gamma$ , some waveforms  $\varphi$  have  $R$ -values and  $c_n$ -values which basically ‘come out even’ (to wit are expressible as simple formulae involving the arithmetic of a quadratic number field such as  $\mathbb{Q}(\sqrt{5})$ ). Yet  $\varphi$  *still* appears to simulate a random wave (cf [12]). Such ‘explicit-type’  $\varphi$  are called Maass waveforms of *CM-type*. We refer to [7, 12] for the technical details of their construction. Suffice it to say here that the coefficients  $c_n$  correspond to a generalization of the idea of a Dirichlet character mod  $k$  and that  $R$  has format  $(\text{const})n\pi/\log \varepsilon$ , where  $\varepsilon$  is the fundamental unit of the relevant real quadratic field  $K$ .

In working with CM-forms, there is no loss of generality if one thinks of their  $\Gamma$  as simply being  $SL(2, \mathbb{Z})$ ; we do so without further comment.

To calculate a Maass waveform at any given  $(x, y)$  to, say, 12 decimal places, one basically needs to use the first  $(\text{const})R/y$  terms in the Fourier ansatz. In the case of a *CM-form*, what is immediately striking (and cause for pause!) is that a significant fraction of the associated  $c_n$  are 0. Clearly, whatever randomness *is* present in  $\varphi$  must reflect those terms which are not zero.

<sup>4</sup> Throughout this paper, we tacitly assume as in [10, section 4] that  $K_{iR}(u)$  has been premultiplied by  $\exp(\frac{\pi}{2}R)$ .

Beyond equidistribution (in the  $L_2$  sense) and a locally Gaussian value distribution<sup>5</sup>, one of the conjectures that grows out of Berry's wider random wave philosophy [6] is that high frequency eigenfunctions should (in a two-dimensional setting) exhibit autocorrelation behaviour which is linked to the standard  $J_0$ -Bessel function

$$J_0(u) = \frac{1}{2\pi} \int_{-\pi}^{\pi} e^{iu \sin \theta} d\theta.$$

In fact<sup>6</sup>, in some *area-averaged* sense, the values of  $\varphi(P)$  and  $\varphi(Q)$  should be correlated such as

$$J_0 \left[ \pi \frac{d(P, Q)}{\delta} \right].$$

Here  $d(P, Q)$  is the shortest-geodesic distance between  $P$  and  $Q$  on  $\mathcal{M}$ . Observe, incidentally, that this Bessel function *does* tend to zero as  $d(P, Q)/\delta$  grows. Indeed

$$J_0(u) \sim \sqrt{\frac{2}{\pi}} \frac{\cos(u - \pi/4)}{\sqrt{u}} \quad \text{as } u \rightarrow \infty.$$

[To avoid topological difficulties, one tacitly assumes in all this that  $d(Q, P) = o(1)$ .]

Thus far, there have been relatively few tests of Berry's conjecture in non-Euclidean settings such as  $\Gamma \backslash H$ , and the overall state-of-affairs remains here somewhat less satisfactory than one would like (in comparison to curvature zero) (cf [1]). Notwithstanding the naturalness of Berry's idea, one wonders, for instance, if<sup>7</sup> the autocorrelation behaviour of CM-forms may possibly differ from that exhibited by 'mock' waveforms  $\hat{\varphi}$  whose coefficients  $\hat{c}_n$  are taken to be random numbers chosen according to some admissible distribution (cf [10, section 6] and [22]; also [13, p 26 (proposition 4.12)] for the *a priori* format).

In its non-Euclidean form, Berry's conjecture refers to taking a generic point  $P$  in some two-dimensional subregion  $S$  of  $\mathcal{M}$  (more precisely,  $\mathcal{M}$ -(its axes of symmetry)) and studying the correlation of  $\varphi(P)$  and  $\varphi(Q)$  for points  $Q$  obtained by letting  $P$  flow in a random direction under the *geodesic* flow for a specified number of seconds. The density function  $\rho(\theta)$  for the  $Q$ -direction can be chosen essentially arbitrarily (cf here [6, equation (7) and (9)] integrated against  $a(q)b(\bar{p})$  using Parseval; also [27, equation (4.6)].)

The machine experiments that we undertook were motivated by a desire to examine the correlation behaviour of CM-forms in some 'thinner' settings where, instead of being restricted to a given *two*-dimensional set  $S$ , the points  $P$  and  $Q$  were constrained to lie along certain rectifiable *arcs*  $\gamma$  and  $\gamma'$ . The essential thing of course is that  $\gamma$  and  $\gamma'$  correspond to one another under some natural correspondence (or flow)—so that there *is* a correlation to be spoken of.

The idea of using  $\gamma$  in place of  $S$  was mentioned earlier in [10, p 295 (bullet 4), 299 (line 21, left)].

To facilitate a comparison with Berry's conjecture, it is clearly best to look at arcs  $\gamma$  and  $\gamma'$  where the corresponding points  $P$  and  $Q$  are located a fixed distance apart.

## 2. Flowing along closed horocycles

Horizontal lines or circles (in  $H$ ) which are tangent to  $\mathbb{R}$  are called horocycles. In the case of a discrete subgroup like  $SL(2, \mathbb{Z})$ , where the point  $i\infty$  is a cusp of width 1, each horocycle  $\{y = y_0\}$  clearly projects onto a closed curve on  $\mathcal{M} = \Gamma \backslash H$ . The hyperbolic length of this

<sup>5</sup> Of mean 0.

<sup>6</sup> On this point, see also the first paragraph of section 5, remark A below.

<sup>7</sup> Due to their *deterministic* nature.

curve is immediately seen to be  $1/y_0$ . (As the length  $1/y_0 \rightarrow \infty$ , the curve is known to become equidistributed on  $\mathcal{M}$  with respect to hyperbolic area (see [14, 24]).)

In contrast to Berry's situation where one flowed along geodesics, we are now interested in taking points  $P = (x, y)$  along an arc  $\gamma$  and passing to  $Q = (x + ty, y)$ ; i.e. flowing along closed horocycles.

Observe incidentally that, as a particle,  $(x_0 + ty_0, y_0)$  traverses  $\{y = y_0\}$  with unit speed in the hyperbolic metric.

Horocycles are not geodesics. Indeed, the hyperbolic distance between  $P$  and  $Q$  on  $H$  is

$$\cosh^{-1} \left( 1 + \frac{t^2}{2} \right)$$

which is always less than  $|t|$ . For small values of  $t$ , the inverse cosh is readily seen to be expandible as

$$|t| \left[ 1 - \frac{1}{24}t^2 + O(t^4) \right].$$

A computer test shows that, at least for  $-1 \leq t \leq 1$ , the implied constant in  $O(t^4)$  can be taken to be the Taylor coefficient  $3/640$  ( $=0.0046875$ ).

So long as  $\gamma$  bypasses any points of ramification of  $\mathcal{M}$  (i.e. elliptic fixpoints), the distance  $d(P, Q)$  on  $\mathcal{M}$  will simply be  $\cosh^{-1}(1 + t^2/2)$ , at least for small  $t$ .

For waveforms with large  $R$ , requiring  $t$  to be small is not a problem, since Berry's conjecture necessitates looking at the ratio  $\frac{d}{\delta} \approx \frac{|t|}{\delta}$ , not  $|t|$ .

What *is* a concern, though, is the length of  $\gamma$ . For simplicity, assume that  $\gamma$  does not cross itself on  $\mathcal{M}$  (i.e. is a Jordan arc). As noted in section 1, waveforms  $\varphi$  begin to manifest 'serious randomness' only at scales bigger than about  $50\delta$  or so; and this was for two-dimensional  $S$ . The comparable number for a one-dimensional setting can only be larger; *how much* larger is not immediately clear (and may conceivably depend on the *geometry* of the given path).

To be on the safe side, whether with  $\varphi$  or  $\hat{\varphi}$ , it clearly makes sense to keep the length of  $\gamma$  bigger than  $50\delta$  or so. Likewise for  $\gamma'$ .

### 3. The experimental set-up

Take  $\Gamma = SL(2, \mathbb{Z})$ . In complex variable notation, the horocyclic flow under discussion is simply

$$\tilde{z} = z + ty.$$

To keep the relation between  $|dz|/y$  and  $|d\tilde{z}|/\text{Im}(\tilde{z})$  transparent, it is natural to look first at arcs  $\gamma$  which are Euclidean line segments. We decided to keep these strictly inside the standard fundamental polygon for  $\Gamma \backslash H$ ; i.e.  $\{|x| < \frac{1}{2}, |z| > 1\}$ .

After some preliminary tests, we chose to restrict the  $y$ -height of  $\gamma$  to be one of three values; namely  $50\delta$ ,  $500\delta$ ,  $1600\delta$ . We also opted to keep the basepoint of  $\gamma$  along the line  $\{y = 1\}$ . (The localizing hypothesis  $d(Q, P) = o(1)$  suggests that this latter choice entails minimal loss of generality in the large  $R$  limit.)

For our CM-forms, we decided to look at:

$$\begin{aligned} R_1 &= 3264.251\ 302\ 636\ 496^+ \\ R_2 &= 25\ 004.164\ 978\ 195\ 566^+ \\ R_3 &= 100\ 016.659\ 912\ 782\ 265^+ \\ R_4 &= 150\ 002.140\ 110\ 054\ 942^+ \end{aligned}$$

The associated  $\varphi$  correspond to the quadratic field  $\mathbb{Q}(\sqrt{5})$  in the notation of [7, 12]<sup>8</sup>.

<sup>8</sup> The stated  $R_j$  are simply  $M\pi/2 \log \varepsilon$  with  $\varepsilon = \frac{1}{2}(1 + \sqrt{5})$  and  $M = 1000, 7660, 30\ 640, 45\ 953$ .

Following [10], in  $\hat{\varphi}(z)$ , we decided to employ  $\hat{c}_n$  chosen (independent randomly) from a uniform distribution on  $[-1, 1]$ . We took two such samplings and used either one or both in forming our mock waveforms. For  $R$ , we simply used the values  $R_1$  and  $R_2$ . (More on this in a moment.)

To ensure about 10-digit accuracy in  $\varphi$  and  $\hat{\varphi}$  along  $\gamma$  and  $\gamma'$ , the following  $n$ -ranges were used in the Fourier development:

(3264)	$1 \leq n \leq 600$
(25 004)	$1 \leq n \leq 4100$
(100 016)	$1 \leq n \leq 16\,100$
(150 002)	$1 \leq n \leq 24\,010$ .

(The upper limit in each case is essentially  $(R + 20R^{1/3})/2\pi$ .) For the associated CM-forms, this produced 137, 799, 2853, 4159 nonzero  $c_n$ , respectively. This ‘reduced’ quantity will be referred to below as  $NZ$ .

From the standpoint of  $NZ$ , the CM-form with  $R = 150\,002^+$  seems most naturally comparable to a mock one with  $R \sim 25\,000$ , the point being here that both depend on about 4100 *nonvanishing* terms.

Because of memory restrictions on our computer, a Cray YMP-EL 4/1024, working out statistics for cases with  $NZ \geq 16\,000$  proved to be unpleasantly cumbersome; we therefore opted to stay with  $NZ \leq 4200$  throughout. This necessitated skipping  $\hat{\varphi}$  with  $R = R_3, R_4$ .

As far as the parameter  $t$  goes, we basically chose to employ

$$\left\{ \begin{array}{l} |t| \leq 250\delta \quad \text{for heights } 50\delta, 500\delta \\ \text{and} \\ |t| \leq 30\delta \quad \text{for height } 1600\delta \end{array} \right\}$$

as our ‘benchmark’ (or, reference) settings. Guided by what we found, the 250 and 30 were then raised in selected cases to permit consideration of a number of  $t$ -intervals of length  $50\delta$  located much farther out. In all instances, the starting  $x$ -value of  $\gamma$  was chosen from among  $\{0.05, 0.06, 0.07\}$  and one was especially interested in looking for autocorrelation behaviour that resembled

$$J_0 \left[ R \cosh^{-1} \left( 1 + \frac{t^2}{2} \right) \right].$$

Cf the  $J_0$  and  $d(P, Q)$  asymptotics in sections 1 and 2.

Since one is dealing with  $C^\infty$  functions, the  $\varphi$  and  $\hat{\varphi}$  correlations necessarily vary continuously with  $t$ . In the ranges considered, it was found that taking  $\Delta t = \frac{1}{10}\delta$  produced a rather good (i.e. ‘smooth’) graph;  $\Delta t = \frac{1}{5}\delta$  a bit less so. To save time, we used  $\frac{1}{5}\delta$ . Any necessary integrals were evaluated using a trapezoid rule with  $\Delta y = \frac{1}{25}\delta$  ( $\frac{1}{15}\delta$  in the case of  $1600\delta$ ). Our calibration tests with  $\Delta y = \frac{1}{50}\delta$  and  $\frac{1}{100}\delta$  showed that, at least heuristically, one was assured of obtaining an additive accuracy of at least three decimal places.

If  $R$  is large *and matters* [in the horocyclic setting] *adhere at all to Berry’s conjecture*, the computed correlations will basically need to oscillate between

$$\pm \frac{\sqrt{2}}{\pi \sqrt{m}}$$

when  $|t| \sim m\delta$  and  $m$  is bigger than about 10. To adhere to the restriction  $d(Q, P) = o(1)$ , one keeps  $m/R \ll 1$ . (Cf also our earlier comment about the arbitrariness of direction-density  $\rho(\theta)$ .)

**Table 1.** Intermediate range correlation statistics.

Configuration	NZ	M	$\langle C \rangle$	$\sigma(C)$	$M^{\text{in}}$	$M^{\text{out}}$	$M^{\text{edge}}$	$\sigma^{\text{in}}$	$\sigma^{\text{out}}$	$\sigma^{\text{edge}}$	$\frac{M}{\sigma(C)}$	$P(2\sigma)$	$P(\frac{3}{2}\sigma)$
3kR	600	0.215	-0.002	0.065	0.183	0.215	0.193	0.072	0.057	0.056	3.31	4.2%	14.0%
3kCM	137	0.229	0.003	0.068	0.206	0.229	0.179	0.071	0.065	0.063	3.37	4.6%	13.9%
25kR	4100	0.272	0.007	0.077	0.272	0.229	0.229	0.080	0.074	0.077	3.53	4.7%	13.3%
25kR(0.5)	4100	0.194	-0.002	0.052	0.194	0.162	0.123	0.056	0.048	0.047	3.73	4.2%	13.8%
25kR(1.0)	4100	0.167	-0.002	0.054	0.167	0.150	0.150	0.056	0.051	0.049	3.09	4.0%	13.4%
25kR̄	4100	0.231	-0.003	0.065	0.223	0.231	0.231	0.069	0.061	0.060	3.55	4.4%	13.2%
150kCM	4159	0.221	0.001	0.065	0.221	0.190	0.190	0.071	0.058	0.053	3.40	5.0%	13.7%
150kCM(0.5)	4159	0.228	0.000	0.062	0.228	0.189	0.157	0.066	0.058	0.054	3.68	4.3%	13.2%
150kCM(1.0)	4159	0.180	-0.001	0.056	0.180	0.173	0.173	0.058	0.054	0.057	3.21	4.3%	13.8%
150kCM <sub>2</sub>	4159	0.263	-0.004	0.073	0.234	0.263	0.212	0.077	0.068	0.069	3.60	4.2%	12.9%
100kCM	2853	0.234	0.002	0.068	0.234	0.194	0.171	0.069	0.066	0.065	3.44	3.8%	14.1%
100kCM <sub>2</sub>	2853	0.241	0.008	0.073	0.241	0.197	0.197	0.081	0.065	0.064	3.30	3.7%	13.4%
25kR(ℓ <sub>o</sub> )	4100	0.407	0.007	0.143	0.407	0.405	0.405	0.140	0.146	0.150	2.85	4.8%	14.6%
25kR̄(ℓ <sub>o</sub> )	4100	0.551	-0.010	0.197	0.518	0.551	0.551	0.194	0.199	0.198	2.80	4.8%	13.3%
150kCM(ℓ <sub>o</sub> )	4159	0.534	0.002	0.163	0.534	0.481	0.481	0.166	0.160	0.157	3.28	4.9%	14.1%
150kCM <sub>2</sub> (ℓ <sub>o</sub> )	4159	0.550	-0.013	0.190	0.550	0.477	0.476	0.194	0.186	0.188	2.89	4.2%	14.3%
25kRe	4100		0.009				0.229			0.077	2.97	4.2%	12.5%
25kRe <sub>2</sub>	4100		-0.008				0.144			0.051	2.82	4.8%	15.3%
25kRe <sub>3</sub>	4100		0.007				0.150			0.061	2.46	3.4%	16.1%
25kR̄e	4100		0.004				0.231			0.060	3.85	5.2%	11.8%
25kR̄e <sub>2</sub>	4100		0.005				0.227			0.072	3.15	3.6%	14.3%
25kR̄e <sub>3</sub>	4100		-0.021				0.174			0.060	2.90	3.6%	11.8%
$\{30\delta \leq  t  \leq 250\delta\} \times \begin{cases} 500\delta & \text{regular} \\ 50\delta & \ell_o \end{cases}$													
								For an initial segment		Inner : $30\delta \leq  t  \leq 140\delta$			
								with $\frac{dx}{dy} = 0$ (or else $\frac{1}{2}, 1$ )		Outer : $140\delta \leq  t  \leq 250\delta$			
										Edge: $200\delta \leq  t  \leq 250\delta$			

**4. Results**

Since a  $1/\sqrt{m}$  decay rate can hardly be missed, we decided to focus in our first series of experiments on ‘larger  $t$ ’, specifically  $30\delta \leq |t| \leq 250\delta$ . (The number 30 was chosen somewhat arbitrarily after running several exploratory jobs at  $R = R_1$  with  $|t| \leq 50\delta$  and height  $50\delta$ , utilizing both  $\varphi$  and  $\hat{\varphi}$ .) Table 1 gives a representative summary of what was found in the case of  $\gamma$ ’s having height either  $50\delta$  or  $500\delta$ .

The following notations are used.  $M$  signifies the correlation of maximum absolute value over the relevant  $t$ -grid with  $\Delta t = \frac{1}{5}\delta$ ;  $\langle C \rangle$  the average correlation;  $\sigma(C)$  the standard deviation.  $P(b\sigma)$  denotes the fraction of those grid-values  $t$  in either  $\{30\delta \leq |t| \leq 250\delta\}$  or  $\{200\delta \leq |t| \leq 250\delta\}$  for which  $|C|$  exceeds  $b\sigma$ . The configurations are coded in a natural way corresponding to  $\sqrt{\lambda - 1/4}$  and the inverse slope of  $\gamma$ .  $R$  indicates use of random sample no 1 for  $\hat{c}_n$ ;  $\bar{R}$  use of no 2. The starting  $x$ -value for  $\gamma$  is 0.07 unless indicated by a subscript; subscript 2 means 0.05; 3 means 0.06. In the last six configurations, the letter ‘ $e$ ’ signifies ‘edge job’.

Several conclusions can be immediately drawn from table 1 vis-à-vis the horocyclic flow.

- (1) In neither the CM *nor* the mock cases does there appear to be any kind of clear adherence to a universal correlation law.
- (2) The correlation behaviour of  $\varphi$  and  $\hat{\varphi}$  in the regular cases seems roughly comparable; likewise in the ‘ $\ell_o$ ’ cases.



**Table 2B.** The comparable data for CM-forms.

Configuration	NZ	M	$\langle C \rangle$	$\sigma(C)$	$M/\sigma$	$P(2\sigma)$	$P(\frac{3}{2}\sigma)$
150kCM9600r	4159	0.151	0.000	0.046	3.28	5.2%	9.6%
150kCM4800r	4159	0.146	-0.004	0.044	3.32	5.2	8.8
150kCM1600r	4159	0.134	0.001	0.061	2.20	1.2	15.9
T150kCM1600r	4159	0.086	0.002	0.039	2.21	3.2	12.4
150kCM800r	4159	0.115	0.004	0.042	2.74	5.6	15.9
T150kCM800r	4159	0.073	0.000	0.029	2.52	3.6	16.3
150kCM250r	4159	0.158	0.007	0.048	3.29	6.8	14.3
T150kCM250r	4159	0.072	0.006	0.028	2.57	2.4	13.9
150kCM250ℓ	4159	0.190	-0.008	0.056	3.39	6.4	12.7
T150kCM250ℓ	4159	0.091	-0.007	0.033	2.76	5.2	11.6
150CM800ℓ	4159	0.156	-0.009	0.059	2.64	5.2	12.7
T150kCM800ℓ	4159	0.102	0.000	0.038	2.68	4.8	12.7
150kCM1600ℓ	4159	0.155	0.003	0.053	2.92	6.4	11.6
T150kCM1600ℓ	4159	0.083	0.005	0.031	2.68	5.2	11.6
150kCM4800ℓ	4159	0.126	-0.003	0.050	2.52	5.6	15.9
150kCM9600ℓ	4159	0.137	0.003	0.052	2.63	4.0%	14.3%

$y_2 - y_1 = 500\delta$  or  $1600\delta$ ; For initial segment with  $\frac{dx}{dy} = 0$  (r) flow to  $0.07 + ty$   
 $t \in [t_1, t_2], t_2 - t_1 = 50\delta$  (ℓ) flow to  $0.07 - ty$

**Table 3A.** Mock form statistics for larger  $t$  and an inclined  $\gamma$ .

Configuration	NZ	M	$\langle C \rangle$	$\sigma(C)$	$M/\sigma$	$P(2\sigma)$	$P(\frac{3}{2}\sigma)$
T25kR1600r(1.0)	4100	0.040	-0.002	0.017	2.35	2.8%	17.5%
T25kR800r(1.0)	4100	0.059	-0.000	0.023	2.57	5.6	15.1
25kR250r(1.0)	4100	0.150	-0.006	0.052	2.88	2.4	13.1
T25kR250r(1.0)	4100	0.085	-0.005	0.035	2.43	2.4	13.5
25kR250ℓ(1.0)	4100	0.131	-0.003	0.045	2.91	4.4	14.7
T25kR250ℓ(1.0)	4100	0.080	-0.003	0.029	2.76	4.4	13.9
T25kR800ℓ(1.0)	4100	0.065	-0.002	0.028	2.32	2.8	13.9
T25kR1600ℓ(1.0)	4100	0.055	-0.002	0.026	2.12	1.2%	16.7%

$y_2 - y_1 = 500\delta$  or  $1600\delta$ ; For initial segment with  $\frac{dx}{dy} = 1$  (r) flow to  $x_0(y) + ty$   
 $t \in [t_1, t_2], t_2 - t_1 = 50\delta$  (ℓ) flow to  $x_0(y) - ty$

**Table 3B.** The comparable data for CM-forms.

Configuration	NZ	M	$\langle C \rangle$	$\sigma(C)$	$M/\sigma$	$P(2\sigma)$	$P(\frac{3}{2}\sigma)$
T150kCM1600r(1.0)	4159	0.074	0.004	0.032	2.31	3.6%	15.1%
T150kCM800r(1.0)	4159	0.063	-0.002	0.025	2.52	3.2	17.1
150kCM250r(1.0)	4159	0.113	-0.003	0.048	2.35	3.6	14.3
T150kCM250r(1.0)	4159	0.102	0.001	0.036	2.83	4.8	15.5
150kCM250ℓ(1.0)	4159	0.173	-0.005	0.064	2.70	1.2	15.9
T150kCM250ℓ(1.0)	4159	0.094	-0.002	0.039	2.41	3.6	12.4
T150kCM800ℓ(1.0)	4159	0.074	0.000	0.026	2.85	3.6	12.0
T150kCM1600ℓ(1.0)	4159	0.052	0.002	0.021	2.48	5.6%	14.7%

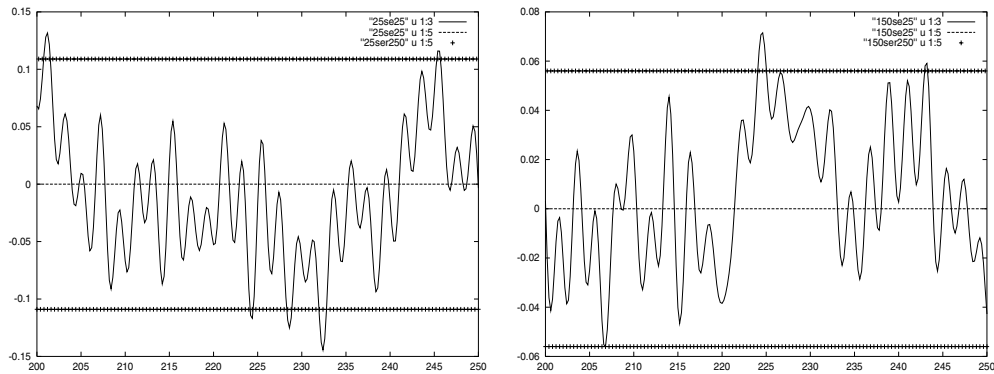
$y_2 - y_1 = 500\delta$  or  $1600\delta$ ; For initial segment with  $\frac{dx}{dy} = 1$  (r) flow to  $x_0(y) + ty$   
 $t \in [t_1, t_2], t_2 - t_1 = 50\delta$  (ℓ) flow to  $x_0(y) - ty$



**Table 4.** Data for a Euclidean variant.

Configuration	NZ	M	$\langle C \rangle$	$\sigma(C)$	$M/\sigma$	$P(2\sigma)$	$(\frac{3}{2}\sigma)$
25kR1600rE	4100	0.186	-0.003	0.078	2.38	1.6%	12.7%
25kR800rE	4100	0.189	-0.023	0.070	2.70	3.6	13.5
25kR800lE	4100	0.238	-0.024	0.080	2.98	5.2	14.7
25kR1600lE	4100	0.137	0.012	0.065	2.11	0.8	13.9
150kCM9600rE	4159	0.150	-0.002	0.060	2.50	5.6	14.3
150kCM4800rE	4159	0.145	-0.009	0.061	2.38	6.0	13.9
150kCM1600rE	4159	0.198	-0.003	0.061	3.25	4.4	13.1
150kCM800rE	4159	0.131	0.002	0.048	2.73	6.4	13.5
150kCM800lE	4159	0.202	-0.012	0.063	3.21	3.6	12.7
150kCM1600lE	4159	0.123	-0.002	0.053	2.32	4.0	15.1
150kCM4800lE	4159	0.138	-0.003	0.055	2.51	6.0	14.3
150kCM9600lE	4159	0.150	0.006	0.060	2.50	2.8	12.7

$y_2 - y_1 = 500\delta;$  For initial segment  $(r)$  flow to  $0.07 + t$   
 $t \in [t_1, t_2], t_2 - t_1 = 50\delta$  with  $\frac{dx}{dy} = 0$   $(l)$  flow to  $0.07 - t$



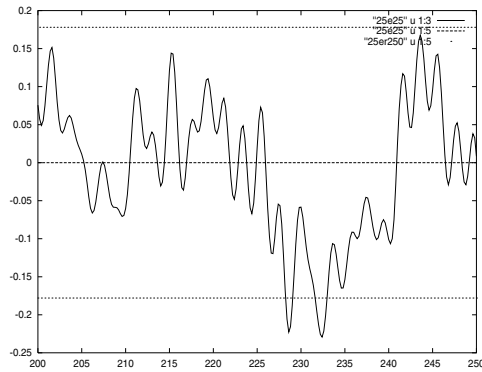
**Figure 1.** Correlation plots for configurations T25kR250r and T150kCM250r in tables 2A and 2B (that is to say: mock and CM-forms having  $R \cong 25k, 150k$ , respectively, a ‘tall’ vertical  $\gamma$ , and  $m$  ranging from 200 to 250). The heights  $\pm 2\sigma(C)$  are indicated. Though the number of peaks and valleys is approximately correct, there is clearly little adherence to a  $\sqrt{2}/\pi \sqrt{m}$  amplitude in either plot. Note too that  $\sqrt{2}/\pi \sqrt{225} = 0.030$ .

Table 4, which features straightforward Euclidean translation, is included mainly for *curiosity’s* sake. It is basically consistent with tables 2–3 and points 1, 2, 3, 5.

To address the possibility in all this that  $C$  may be being unduly affected by some lack of equidistribution (in the  $L_2$  sense) along the one-dimensional arcs  $\gamma$  and  $\gamma'$ , we performed a number of further tests. One was simply to redefine the correlation  $C$  to have schematic format  $I/s(0)^2$  instead of  $I/s(0)s(t)$ . This typically produced only modest changes in the  $M$  and  $\sigma(C)$  values over the respective intervals, and, in particular, no essential changes in points 1–5.

In tables 5A–5D, using an obvious shorthand, we indicate *the mean and standard deviation* of the average and root mean square of  $\varphi$  (or  $\hat{\varphi}$ ) taken along  $\gamma'$  with respect to  $|d\tilde{z}|/\text{Im}(\tilde{z})$  for each of our configurations. (The final columns gives the corresponding data for  $\gamma$ .)

The values for the root mean square of  $\varphi(\hat{\varphi})$  compare quite favourably, in fact, with the heuristic  $\sqrt{\frac{\pi}{8}}\Omega$  discussed in [10, section 6] (especially if the ‘ $\ell o$ ’ configurations are omitted).



**Figure 2.** Correlation plot for (mock, regular) configuration 25kR250r in table 2A. The very light dotted lines depict  $\pm 2\sigma(C)$ . The increase seen in  $\sigma(C)$  (from 0.055 to 0.089) as the length of  $\gamma$  is reduced from 1600 $\delta$  to 500 $\delta$  is typical.

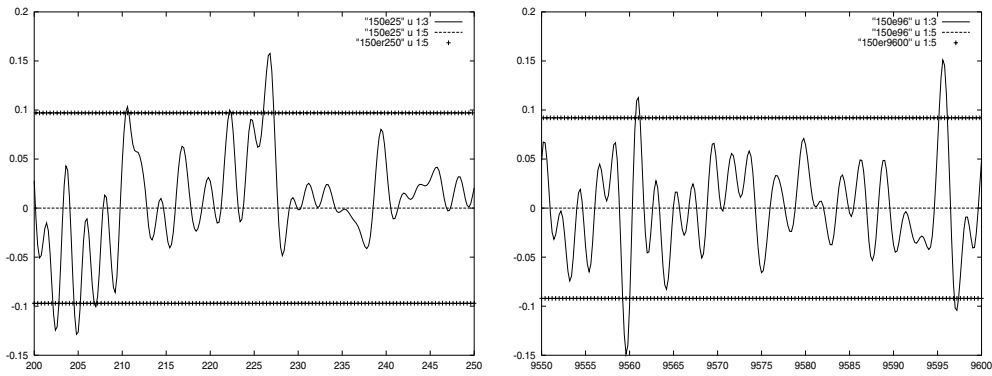


**Figure 3.** Correlation plots for (regular) configurations 150kCM250r and 150kCM9600r in table 2B. The heights  $\pm 2\sigma(C)$  ( $=\pm 0.096, \pm 0.092$ ) are indicated. Observe that the general texture in these plots is similar even though, in the second one,  $m$  is over 38 times bigger.

One computes

$$\Omega = \frac{1}{X} \sum_{n \leq X} |c_n|^2 \quad \left( \text{or } \frac{1}{X} \sum_{n \leq X} |\hat{c}_n|^2 \right)$$

for  $X$ -values approximately equal to the upper limit stated in paragraph 5 of section 3, and then forms the associated  $\sqrt{\pi\Omega/8}$ . The latter do not vary all that much. In this way, the heuristically expected ‘ideal’ RMS-values are found to conservatively be

- $0.359 \pm 0.003$  for 3kR
- $0.430 \pm 0.003$  for 3kCM
- $0.358 \pm 0.002$  for 25kR\* cases
- $0.366 \pm 0.002$  for 25kR̄\* cases
- $0.443 \pm 0.002$  for 100kCM\* cases
- $0.419 \pm 0.001$  for 150kCM\* cases.

**Table 5A.** Waveform fluctuation data corresponding to table 1.

Configuration	Average	R.M.S.	$\sqrt{\frac{\pi}{8}\Omega}$	For $\gamma$
$3kR[\pm 30, \pm 250]$	$0.000 \pm 0.003$	$0.358 \pm 0.014$	0.359	(0.003, 0.320)
$3kCM[\pm 30, \pm 250]$	$0.000 \pm 0.012$	$0.428 \pm 0.018$	0.430	(0.013, 0.443)
$25kR[*]$	$0.000 \pm 0.007$	$0.347 \pm 0.015$	0.358	(-0.008, 0.366)
$25kR(0.5)[*]$	$0.000 \pm 0.017$	$0.352 \pm 0.015$	0.358	(-0.023, 0.344)
$25kR(1.0)[*]$	$0.000 \pm 0.005$	$0.349 \pm 0.010$	0.358	(-0.008, 0.357)
$25k\bar{R}[*]$	$0.000 \pm 0.004$	$0.363 \pm 0.013$	0.366	(0.001, 0.374)
$150kCM[*]$	$0.000 \pm 0.002$	$0.423 \pm 0.015$	0.419	(0.001, 0.421)
$150kCM(0.5)[*]$	$0.000 \pm 0.020$	$0.428 \pm 0.015$	0.419	(0.019, 0.423)
$150kCM(1.0)[*]$	$0.000 \pm 0.008$	$0.435 \pm 0.014$	0.419	(-0.009, 0.397)
$150kCM_2[*]$	$0.000 \pm 0.015$	$0.419 \pm 0.017$	0.419	(-0.002, 0.349)
$100kCM[*]$	$0.000 \pm 0.016$	$0.435 \pm 0.017$	0.443	(-0.017, 0.442)
$100kCM_2[*]$	$0.000 \pm 0.001$	$0.429 \pm 0.019$	0.443	(-0.000, 0.486)
$25kR(\ell o)[*]$	$0.000 \pm 0.014$	$0.338 \pm 0.040$	0.358	(-0.007, 0.317)
$25k\bar{R}(\ell o)[*]$	$0.000 \pm 0.090$	$0.355 \pm 0.042$	0.366	(-0.033, 0.344)
$150kCM(\ell o)[*]$	$0.000 \pm 0.048$	$0.420 \pm 0.048$	0.419	(-0.072, 0.492)
$150kCM_2(\ell o)[*]$	$0.000 \pm 0.019$	$0.427 \pm 0.053$	0.419	(-0.009, 0.446)
$25kRe[\pm 200, \pm 250]$	$0.000 \pm 0.007$	$0.359 \pm 0.017$	0.358	(-0.008, 0.366)
$25kRe_2[*]$	$0.000 \pm 0.006$	$0.336 \pm 0.011$	0.358	(0.009, 0.347)
$25kRe_3[*]$	$0.000 \pm 0.009$	$0.345 \pm 0.012$	0.358	(0.006, 0.337)
$25k\bar{R}e[*]$	$0.000 \pm 0.005$	$0.356 \pm 0.013$	0.366	(0.001, 0.374)
$25k\bar{R}e_2[*]$	$0.000 \pm 0.011$	$0.364 \pm 0.015$	0.366	(0.015, 0.379)
$25k\bar{R}e_3[*]$	$0.000 \pm 0.023$	$0.357 \pm 0.013$	0.366	(0.013, 0.360)

In each instance, one knows from [10, section 6] (and Fubini’s theorem) that an additive error of  $O(1)R^{-1/3}$  is more or less inevitable in the RMS values. We remark here that

$$R_1^{-\frac{1}{3}} = 0.067 \quad R_2^{-\frac{1}{3}} = 0.034 \quad R_3^{-\frac{1}{3}} = 0.022 \quad R_4^{-\frac{1}{3}} = 0.019$$

and that the likely implied constant in  $O(1)$  can be shown (by a *heuristic* calculation based on [10, equations (2.3), (2.4)] and [20]) to be at most  $2\sqrt{\pi\Omega/8}$ .

The upshot, of course, is that in *all* our configurations (except possibly the ‘ $\ell o$ ’ ones), it is fair to say that equidistribution is seen to be taking hold in a generally robust manner along the various arcs  $\gamma'$ .

This is reassuring not only for the calculation of  $C$ , but also intrinsically (cf [10, p 299 (line 21, left)]).

Our results about  $C$  in the range  $|t| \geq 30\delta$  clearly raise a host of further questions eminently suitable for investigation in a later paper; see section 5 for some additional comments concerning this.

We now shift our focus to ‘smaller  $t$ ’; i.e.  $|t| \leq 30\delta$ . Here the situation apropos Berry’s conjecture turns out to be much more satisfactory.

Let  $D(t) = |C(t) - J_0[R \cosh^{-1}(1 + \frac{1}{2}t^2)]|$ . Table 6 shows the mean and maximum values of  $D(t)$  taken over the usual  $\frac{1}{5}\delta$ -grid on either  $\{|t| \leq 6\delta\}$  or  $\{|t| \leq 30\delta\}$  for a variety of configurations. (For scaling purposes, observe that  $\sqrt{2}/\pi\sqrt{m} = 0.18, 0.12, 0.08$  when  $m = 6, 15$  and  $30$ .)

Once again, there is a manifest tendency for the fit to improve as the length of  $\gamma$  goes up. The utility of examining  $D(t)$  over *both*  $\{|t| \leq 6\delta\}$  and  $\{|t| \leq 30\delta\}$  naturally seems highest in the ‘tall’ (i.e.  $T$ ) cases, particularly given points 3 through 5 in the  $|t| \geq 30\delta$

setting. In particular: note that the slight anomaly exhibited by configuration T150kCM(1.0) on  $\{|t| \leq 6\delta\}$  basically ‘corrects itself’ over  $\{|t| \leq 30\delta\}$ .

Observe too that the fits for  $R = 25\,004^+(\hat{\varphi})$  and  $R = 150\,002^+(\varphi)$  are roughly comparable throughout the ‘ $\ell o$ ’, regular, and ‘tall’ settings.

See figures 4–9 for some representative plots of  $C(t)$  versus  $J_0[R \cosh^{-1}(1 + \frac{1}{2}t^2)]$ .

Particularly on the basis of the  $T$ -configurations, it seems reasonable to say that, in the present horocyclic setting,

*$C(t)$  does finally appear to be converging as  $R \rightarrow \infty$  to  $J_0[R \cosh^{-1}(1 + \frac{1}{2}t^2)]$  albeit rather slowly (not only in regard to  $|t|/\delta$ , but also the length of  $\gamma$ ).*

Just as with  $|t| \geq 30\delta$ , there is clearly room here (not to mention need!) for a variety of further experiments.

The bulk of our results were obtained by running microtasked vectorized code on all 4 processors of Uppsala’s Cray YMP-EL. The availability of greater memory and a larger number of processors would have enabled us to go much further. A typical runtime for one of our ‘T’ jobs on  $[-30\delta, 30\delta]$  was  $3.93 \times 8.71 \text{ h} = 34.23 \text{ h}$ .

**Table 5B.** Corresponding to table 2.

Configuration	Average	R.M.S.	$\sqrt{\frac{\pi}{8}}\Omega$	For $\gamma$
25kR1600r	0.000 ± 0.010	0.364 ± 0.014	0.358	(−0.008, 0.366)
T25kR1600r	0.000 ± 0.011	0.361 ± 0.006	0.358	(−0.000, 0.359)
25kR800r	0.000 ± 0.007	0.362 ± 0.011	0.358	(−0.008, 0.366)
T25kR800r	0.000 ± 0.012	0.368 ± 0.005	0.358	(−0.000, 0.359)
25kR250r	0.000 ± 0.007	0.367 ± 0.017	0.358	(−0.008, 0.366)
T25kR250r	0.000 ± 0.011	0.358 ± 0.008	0.358	(−0.000, 0.359)
25kR250ℓ	0.000 ± 0.007	0.351 ± 0.014	0.358	(−0.008, 0.366)
T25kR250ℓ	0.000 ± 0.011	0.353 ± 0.007	0.358	(−0.000, 0.359)
25kR800ℓ	0.000 ± 0.007	0.342 ± 0.013	0.358	(−0.008, 0.366)
T25kR800ℓ	0.000 ± 0.012	0.351 ± 0.007	0.358	(−0.000, 0.359)
25kR1600ℓ	0.000 ± 0.012	0.349 ± 0.012	0.358	(−0.008, 0.366)
T25kR1600ℓ	0.000 ± 0.010	0.358 ± 0.006	0.358	(−0.000, 0.359)
150kCM9600r	0.000 ± 0.013	0.406 ± 0.014	0.419	(0.001, 0.421)
150kCM4800r	0.000 ± 0.006	0.434 ± 0.016	0.419	(0.001, 0.421)
150kCM1600r	0.000 ± 0.002	0.420 ± 0.013	0.419	(0.001, 0.421)
T150kCM1600r	0.000 ± 0.005	0.419 ± 0.006	0.419	(−0.004, 0.410)
150kCM800r	0.000 ± 0.004	0.426 ± 0.017	0.419	(0.001, 0.421)
T150kCM800r	0.000 ± 0.007	0.423 ± 0.007	0.419	(−0.004, 0.410)
150kCM250r	0.000 ± 0.001	0.425 ± 0.014	0.419	(0.001, 0.421)
T150kCM250r	0.000 ± 0.006	0.419 ± 0.008	0.419	(−0.004, 0.410)
150kCM250ℓ	0.000 ± 0.004	0.416 ± 0.013	0.419	(0.001, 0.421)
T150kCM250ℓ	0.000 ± 0.007	0.414 ± 0.007	0.419	(−0.004, 0.410)
150kCM800ℓ	0.000 ± 0.002	0.420 ± 0.014	0.419	(0.001, 0.421)
T150kCM800ℓ	0.000 ± 0.006	0.420 ± 0.007	0.419	(−0.004, 0.410)
150kCM1600ℓ	0.000 ± 0.005	0.402 ± 0.009	0.419	(0.001, 0.421)
T150kCM1600ℓ	0.000 ± 0.006	0.412 ± 0.006	0.419	(−0.004, 0.410)
150kCM4800ℓ	0.000 ± 0.011	0.439 ± 0.019	0.419	(0.001, 0.421)
150kCM9600ℓ	0.000 ± 0.007	0.400 ± 0.011	0.419	(0.001, 0.421)

**Table 5C.** Corresponding to table 3.

Configuration	Average	R.M.S.	$\sqrt{\frac{\pi}{8}\Omega}$	For $\gamma$
$T25kR1600r(1.0)$	$0.000 \pm 0.004$	$0.374 \pm 0.008$	0.358	(−0.001, 0.355)
$T25kR800r(1.0)$	$0.000 \pm 0.003$	$0.355 \pm 0.005$	0.358	(−0.001, 0.355)
$25kR250r(1.0)$	$0.000 \pm 0.005$	$0.352 \pm 0.010$	0.358	(−0.008, 0.357)
$T25kR250r(1.0)$	$0.000 \pm 0.003$	$0.350 \pm 0.005$	0.358	(−0.001, 0.355)
$25kR250\ell(1.0)$	$0.000 \pm 0.008$	$0.341 \pm 0.007$	0.358	(−0.008, 0.357)
$T25kR250\ell(1.0)$	$0.000 \pm 0.007$	$0.354 \pm 0.004$	0.358	(−0.001, 0.355)
$T25kR800\ell(1.0)$	$0.000 \pm 0.006$	$0.350 \pm 0.005$	0.358	(−0.001, 0.355)
$T25kR1600\ell(1.0)$	$0.000 \pm 0.005$	$0.357 \pm 0.005$	0.358	(−0.001, 0.355)
$T150kCM1600r(1.0)$	$0.000 \pm 0.001$	$0.415 \pm 0.006$	0.419	(0.006, 0.416)
$T150kCM800r(1.0)$	$0.000 \pm 0.005$	$0.418 \pm 0.006$	0.419	(0.006, 0.416)
$150kCM250r(1.0)$	$0.000 \pm 0.010$	$0.432 \pm 0.017$	0.419	(−0.009, 0.397)
$T150kCM250r(1.0)$	$0.000 \pm 0.006$	$0.440 \pm 0.008$	0.419	(0.006, 0.416)
$150kCM250\ell(1.0)$	$0.000 \pm 0.002$	$0.443 \pm 0.017$	0.419	(−0.009, 0.397)
$T150kCM250\ell(1.0)$	$0.000 \pm 0.005$	$0.426 \pm 0.007$	0.419	(0.006, 0.416)
$T150kCM800\ell(1.0)$	$0.000 \pm 0.009$	$0.422 \pm 0.009$	0.419	(0.006, 0.416)
$T150kCM1600\ell(1.0)$	$0.000 \pm 0.008$	$0.409 \pm 0.004$	0.419	(0.006, 0.416)

**Table 5D.** And, finally, corresponding to table 4.

Configuration	Average	R.M.S.	$\sqrt{\frac{\pi}{8}\Omega}$	For $\gamma$
$25kR1600rE$	$0.000 \pm 0.011$	$0.361 \pm 0.010$	0.358	(−0.008, 0.366)
$25kR800rE$	$0.000 \pm 0.010$	$0.361 \pm 0.009$	0.358	(−0.008, 0.366)
$25kR800\ell E$	$0.000 \pm 0.010$	$0.340 \pm 0.011$	0.358	(−0.008, 0.366)
$25kR1600\ell E$	$0.000 \pm 0.011$	$0.351 \pm 0.008$	0.358	(−0.008, 0.366)
$150kCM9600rE$	$0.000 \pm 0.022$	$0.413 \pm 0.015$	0.419	(0.001, 0.421)
$150kCM4800rE$	$0.000 \pm 0.013$	$0.431 \pm 0.015$	0.419	(0.001, 0.421)
$150kCM1600rE$	$0.000 \pm 0.026$	$0.416 \pm 0.012$	0.419	(0.001, 0.421)
$150kCM800rE$	$0.000 \pm 0.021$	$0.424 \pm 0.018$	0.419	(0.001, 0.421)
$150kCM800\ell E$	$0.000 \pm 0.006$	$0.421 \pm 0.014$	0.419	(0.001, 0.421)
$150kCM1600\ell E$	$0.000 \pm 0.024$	$0.404 \pm 0.013$	0.419	(0.001, 0.421)
$150kCM4800\ell E$	$0.000 \pm 0.002$	$0.431 \pm 0.015$	0.419	(0.001, 0.421)
$150kCM9600\ell E$	$0.000 \pm 0.010$	$0.408 \pm 0.010$	0.419	(0.001, 0.421)

## 5. Remarks

To better understand the foregoing results, we need to make a number of comments.

- (A) One knows that, in Euclidean space, the Berry autocorrelation conjecture is a consequence of the (more general) Berry–Voros hypothesis concerning the limiting behaviour of the spatially averaged Wigner function  $\bar{\Psi}(q, p)$  (cf [6, equations (9), (20), (21)]; also [21, section 8.1]). In *hyperbolic space*, however, the geometry is different and the implication is not so clear.

At least in the case of a uniform density  $\rho(\theta) = 1/2\pi$ , (the area-averaged form of) Berry’s conjecture turns out to be rather easily derivable from *quantum unique ergodicity* on  $\mathcal{M}$ ; i.e. wavefunction equidistribution in the  $L_2$  sense.

To see this, it suffices to work locally on  $\mathcal{M}$ , hence  $H$ . To define  $\theta$  consistently about each non-ramified testpoint  $z_0$ , one writes

$$i \frac{z - z_0}{z - \bar{z}_0} = r e^{i\theta}.$$

The affine map  $z = y_0 w + x_0$  will then pull things back to the standard geodesic polar coordinate system at  $i$ . As usual

$$r = \tanh \frac{d(z, z_0)}{2}.$$

**Table 6.** Mean/max values for  $D(t)$ .

Configuration	$ t  \leq 6\delta$	$ t  \leq 30\delta$
$3kR$	(0.097, 0.249)	
$3kCM$	(0.060, 0.216)	
$25kR$	(0.080, 0.253)	(0.089, 0.297)
$T25kR$	(0.047, 0.107)	(0.046, 0.151)
$25kR(0.5)$	(0.036, 0.117)	(0.039, 0.126)
$T25kR(0.5)$	(0.024, 0.084)	(0.027, 0.084)
$25kR(1.0)$	(0.035, 0.092)	(0.040, 0.121)
$T25kR(1.0)$	(0.019, 0.052)	(0.022, 0.079)
$25k\bar{R}$	(0.041, 0.111)	
$150kCM$	(0.063, 0.142)	(0.056, 0.173)
$T150kCM$	(0.036, 0.085)	(0.035, 0.115)
$150kCM(0.5)$	(0.049, 0.133)	(0.043, 0.133)
$T150kCM(0.5)$	(0.023, 0.055)	(0.026, 0.071)
$150kCM(1.0)$	(0.037, 0.092)	(0.041, 0.131)
$T150kCM(1.0)$	(0.035, 0.093)	(0.029, 0.093)
$150kCM_2$	(0.052, 0.161)	
$100kCM$	(0.038, 0.127)	
$100kCM_2$	(0.045, 0.138)	
$25kR(\ell_0)$	(0.222, 0.518)	
$25k\bar{R}(\ell_0)$	(0.152, 0.368)	
$150kCM(\ell_0)$	(0.133, 0.447)	
$150kCM_2(\ell_0)$	(0.222, 0.439)	

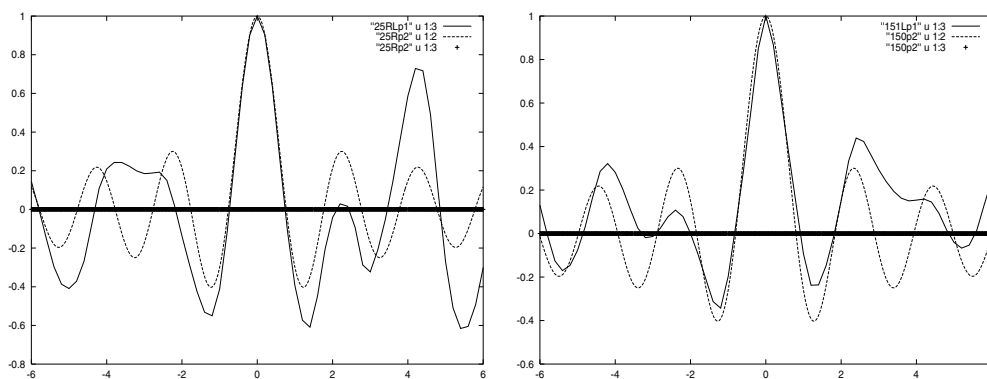


**Figure 4.** Correlation plots for configurations  $25kR(\ell_0)$ ,  $150kCM(\ell_0)$  over  $\{|t| \leq 6\delta\}$ . The lighter curve is  $J_0[R \cosh^{-1}(1 + t^2/2)]$ .

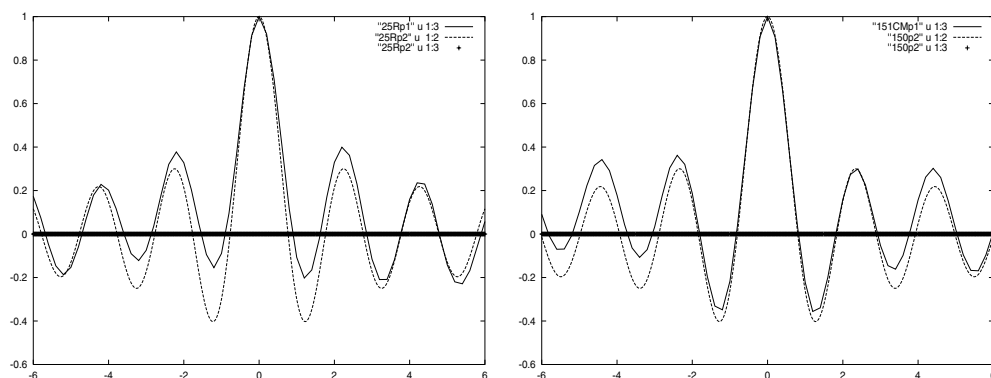


Figure 5. The same as figure 4 but for (regular) configurations 25kR, 150kCM.

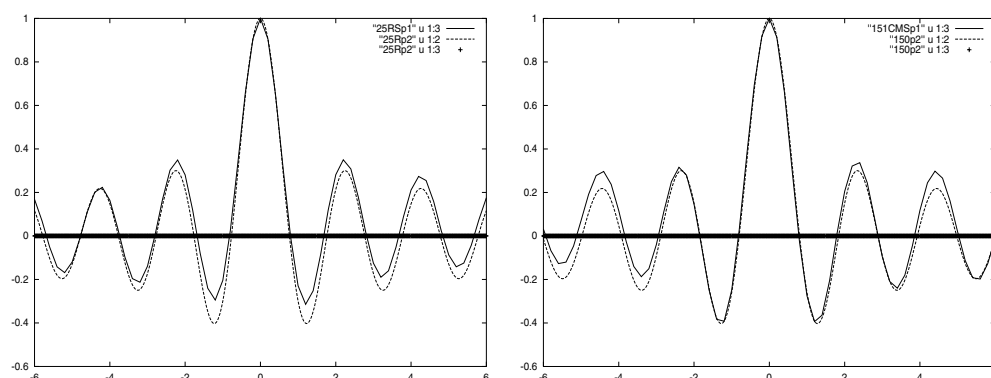


Figure 6. Correlation plots for (tall) configurations T25kR, T150kCM.

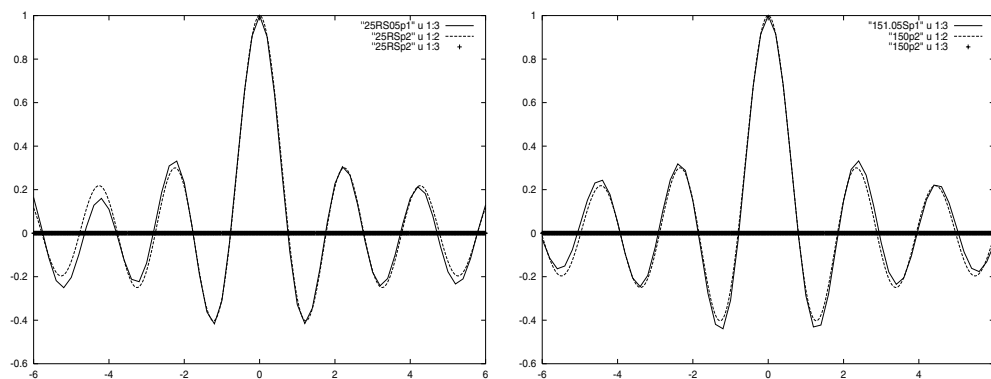


Figure 7. Correlation plots for (tall) configurations T25kR(0.5), T150kCM(0.5).

Let  $\varphi(x, y)$  be any square integrable wavefunction on  $\mathcal{M}$  with eigenvalue  $\lambda = \frac{1}{4} + R^2$ . The quantity we need to compute is

$$C(m) = \frac{\int_S \int_0^{2\pi} \varphi(z_0) \psi(r e^{i\theta}) \rho(\theta) d\theta dA}{\left\{ \int_S \int_0^{2\pi} \varphi(z_0)^2 \rho(\theta) d\theta dA \right\}^{1/2} \left\{ \int_S \int_0^{2\pi} \psi(r e^{i\theta})^2 \rho(\theta) d\theta dA \right\}^{1/2}}$$

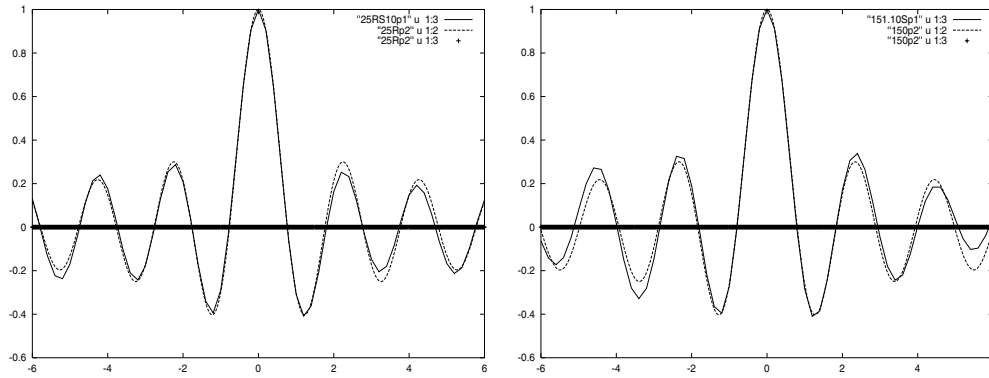


Figure 8. Correlation plots for (tall) configurations T25kR(1.0), T150kCM(1.0).

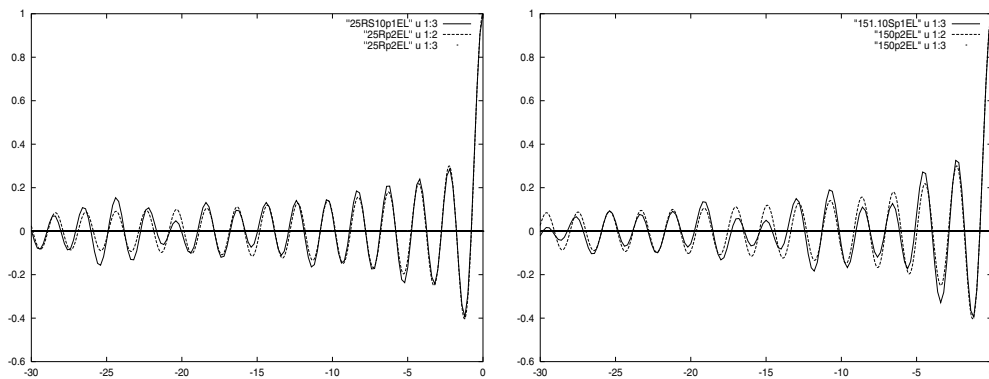


Figure 9A. Correlation plots for (tall) configurations T25kR(1.0), T150kCM(1.0) over the bigger interval  $\{-30\delta \leq t \leq 0\}$ . The lighter curve is again  $J_0[R \cosh^{-1}(1 + t^2/2)]$ .

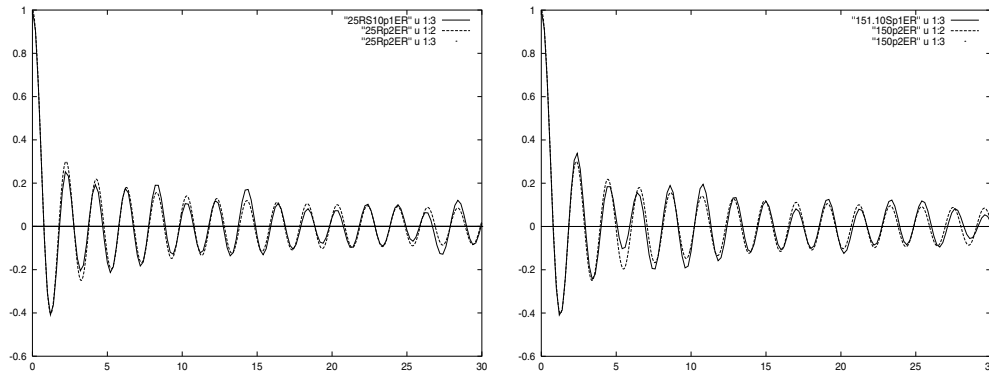


Figure 9B. Correlation plots for (tall) configurations T25kR(1.0), T150kCM(1.0) over  $\{0 \leq t \leq 30\delta\}$ .

where  $r = \tanh(m\delta/2)$ ,  $dA = y_0^{-2} dx_0 dy_0$ ,  $\psi$  is the obvious  $z_0$ -transplant of  $\varphi$ , and  $S$  is some small two-dimensional subregion of  $\mathcal{M}$ . There is no loss of generality if we take the  $L_2$  norm of  $\varphi$  to be 1; we do so. A simple calculation using QUE and the affine map



$z = y_0 w + x_0$  shows that the denominator is asymptotic to  $A(S)/A(\mathcal{M})$  for each  $m > 0$  (and, in fact, any  $\rho$ ). In the numerator, one finds using [13, p 21 (line 7)] that

$$\int_0^{2\pi} \psi(r e^{i\theta}) \rho(\theta) d\theta = \frac{1}{2\pi} \int_0^{2\pi} \psi(r e^{i\theta}) d\theta = \varphi(z_0) F\left(\frac{1}{2} - iR, \frac{1}{2} + iR; 1; \frac{r^2}{r^2 - 1}\right). \tag{5.1}$$

We thus have

$$C(m) \sim F\left[\frac{1}{2} + iR, \frac{1}{2} - iR; 1; -\sinh^2(m\delta/2)\right].$$

To connect things with  $J_0$ , we use the elementary fact that

$$\lim_{R \rightarrow \infty} F\left(\frac{1}{2} - iR, \frac{1}{2} + iR; 1; -\frac{u^2}{4R^2 + 1}\right) = J_0(u) \tag{5.2}$$

holds uniformly over compact subsets of  $\mathbb{C}$  (see [28, pp 154, 155])<sup>9</sup>. This gives  $C(m) \sim J_0(\pi m)$ , exactly as expected<sup>10</sup> (compare [1, p 210]).

The case of more general density functions  $\rho$  can presumably be pushed through using an appropriate pseudodifferential operator variant of QUE. In this regard cf [3, equations (13), (16), (19)], [5, equations (28) and (31)], [9, equation (23)], (5.1), [13, p 21 (lines 4–8)] and [27, equation (4.6)].

- (B) In line with [13, p 21], it is natural to think of  $\psi(r e^{i\theta}) = \varphi(y_0 w + x_0)$  in  $C(m)$  as being written

$$\varphi(z_0) F\left(\frac{1}{2} - iR, \frac{1}{2} + iR; 1; \frac{r^2}{r^2 - 1}\right) + \llbracket \text{remainder} \rrbracket.$$

The function  $\varphi(z_0)\llbracket \text{remainder} \rrbracket$  is reminiscent of the distribution  $dU_j$  considered in [29, pp 8, 9] (see [29, p 25 (3.6)], [17, p 1479] and [15] for some additional perspectives).

The foregoing decomposition and the discussion in (A) suggest that the appearance of  $J_0$  in our experiments for  $d/\delta$  small is most likely a manifestation of (5.2) and an appropriate one-dimensional  $\Psi DO$  form of QUE being true—at least in the CM and mock settings.

To better appreciate this, observe that, for  $m > 0$ , the horocyclic flow

$$\tilde{z} = z + (m\delta)y$$

taking  $\gamma$  onto  $\gamma'$  is pointwise equivalent to a geodesic flow inclined at angle  $\arctan(\frac{1}{2}t)$ , where  $t = m\delta$ . Similarly for  $m < 0$ . One is thus dealing, in the  $\gamma$ -analogue of  $C(m)$ , with density functions  $\rho$  which are effectively Dirac deltas having a ‘sliding’ centre.

In this regard, see also the  $O(1)R^{-1/3}$  heuristic mentioned in connection with tables 5A–5D (column 3).

- (C) As  $R \rightarrow \infty$ , it is tempting to try to replace the ‘sliding’ deltas with fixed ones. To this end, let  $\zeta$  temporarily denote the point obtained by flowing to the right along the *horizontally* directed geodesic at  $z$  a distance of  $t$  units. One readily checks that

$$\zeta = \tilde{z} + yO(t^2)$$

for  $|t| < 1$ . Upon setting  $t = m\delta$  and remembering that  $\text{grad } \varphi = O(R)$  (at least heuristically), we immediately see that

$$\varphi(\zeta) = \varphi(\tilde{z}) + O\left(\frac{m^2}{R}\right). \tag{5.3}$$

<sup>9</sup> The rate of convergence in (5.2) naturally slows down as  $|u|$  grows.

<sup>10</sup> Note too that when  $\varphi$  is of CM-type, QUE is a theorem (cf [16, 25]).

In this light, the results in section 4 for  $d/\delta$  small can be equivalently interpreted as supporting the ‘ $\gamma$ -theoretic’ version of the *usual* Berry conjecture with  $\rho = \delta(\theta - n\pi)$ .<sup>11</sup>

- (D) In section 3 paragraph 2, we suggested that taking a  $y = 1$  baseline entails minimal loss of generality for large  $R$ —a fact that seems eminently reasonable if the relevant  $\varphi$  (and  $\hat{\varphi}$ ) are viewed as *formal* Fourier developments à la [10, section 6] and the  $H$ -lengths of  $\gamma$  and  $\gamma'$  are kept small<sup>12</sup>.

To the extent that  $y = 1$  and  $y = y_0$  do produce similar behaviour, it is natural to contemplate taking  $y_0$  successively smaller (in steps) so that the pull-back of  $\{y = y_0\}$  to the standard fundamental polygon  $\mathcal{F}$  of  $SL(2, \mathbb{Z}) \backslash H$  becomes ever more dense *at the level of phase space*. Cf [24] for this last point.

Insofar as  $d/\delta$  and  $\ell(\gamma)/\delta$  are both kept bounded, one is quickly led to the *expectation* that, at least for ‘true’  $\varphi$ , results akin to those in section 4 should be found for flows in  $\mathcal{F}$  (either geodesic or horocyclic!) which start out at an *arbitrary* angle of inclination.

The essential point in this is that the pull-back mappings are all (conformal) isometries, which enables an analogue of (5.3) to be derived *on a case-by-case basis*, since in each

$$\begin{aligned} & \text{(a ‘radius’ of } m\delta) \cdot [\text{a maximal angular variation of } O(1)\ell(\gamma)] \\ &= (m\delta)O(1)\delta = O(1)mR^{-2}. \end{aligned}$$

Needless to say: some further experiments exploring this heuristic expectation would naturally be very useful (not just for *CM*-cases, but also Maass forms of ‘generic’ type).

In *mock* settings, one fully expects the same independence of direction to be seen in any experiment. Here, however, the emphasis is a bit different—and supplying a rigorous *proof* for things (in the spirit, say, of [22]) may not be entirely out of the question.

- (E) The  $O(1)R^{-1/3}$  heuristic mentioned in connection with table 5’s RMS-entries is obtained by making a natural approximation to the sum

$$\frac{1}{2} \sum_{n \leq M} |c_n|^2 y K_{iR}(2\pi ny)^2 \quad ([10, \text{equation (6.6)}])$$

based on [20]. Along the way, three important sources of error are simply ignored; namely

- (i) the effect of replacing  $[0, \frac{1}{2}]$  in [22] by a much shorter interval  $[x_1, x_2]$ ;
- (ii) the contribution from  $r(u) \equiv \sum_{n \leq u} |c_n|^2 - \Omega u$ ;
- (iii) the contribution from the generalized trigonometric sum cited in [10, p 297 (line-9, left)].

By using the same *idea* but a more careful treatment of  $K_{iR}(2\pi ny)^2$  based on the identity

$$\int_x^\infty Ai(t)^2 dt = Ai'(x)^2 - x Ai(x)^2 \quad (5.4)$$

one is able to replace  $O(1)R^{-1/3}$  by

$$O(1)\sqrt{\frac{\log R}{R}}.$$

This new heuristic is interesting because it is essentially identical with the  $O(R^{-\frac{1}{2}+\epsilon})$  bound obtained by Luo and Sarnak [19] in spectrally averaged two-dimensional ‘macroscopic’ (non de Broglie) settings over  $SL(2, \mathbb{Z}) \backslash H$ . In this regard, see also [2] and [8]. Reference [8] includes a suggestive link with random matrix theory.

<sup>11</sup> The use of  $z = y_0 w + x_0$  being tacitly understood.

<sup>12</sup> The latter condition guarantees that the set of ‘active’  $c_n(\hat{c}_n)$  remains relatively fixed.

- (F) Our final comment pertains to the ‘saturated noise levels’ found in tables 1–4 (cf point 5 in section 4) and is prompted in part by the aforementioned  $O(R^{-\frac{1}{2}+\varepsilon})$  bound of Luo/Sarnak. Namely, as the ratio  $\ell(\gamma)/\delta$  is taken successively larger, *one wonders* what happens to the saturated noise level as a function of  $R$ . Likewise if  $\ell(\gamma)/\delta$  is allowed to grow, say, like a small power of  $R$ .

In both cases, the probable answer is not immediately clear and some further numerical experimentation may well prove useful (compare [26] and [5, section 4.1]).

## Acknowledgments

The results in this paper grew out of some preliminary calculations done by HC during the term of his undergraduate research participation award at the University of Minnesota. We are grateful to Holger Then of Ulm for drawing our attention to (5.4). DH’s work was supported in part by an EU grant on the mathematical aspects of quantum chaos.

## References

- [1] Aurich R and Steiner F 1993 Statistical properties of highly excited quantum eigenstates of a strongly chaotic system *Physica D* **64** 185–214
- [2] Aurich R and Taglieber M 1998 On the rate of quantum ergodicity on hyperbolic surfaces and for billiards *Physica D* **118** 84–102
- [3] Bäcker A, Schubert R and Stifter P 1998 Rate of quantum ergodicity in Euclidean billiards *Phys. Rev. E* **57** 5425–47
- [4] Bäcker A and Schubert R 2002 Amplitude distribution of eigenfunctions in mixed systems *J. Phys. A: Math. Gen.* **35** 527–38
- Bäcker A and Schubert R 1999 *Physica D* **129** 1–14
- [5] Bäcker A and Schubert R 2002 Autocorrelation function of eigenstates in chaotic and mixed systems *J. Phys. A: Math. Gen.* **35** 539–64
- [6] Berry M V 1977 Regular and irregular semiclassical wavefunctions *J. Phys. A: Math. Gen.* **10** 2083–91
- [7] Bump D 1996 *Automorphic Forms and Representations* (Cambridge: Cambridge University Press) p 112ff
- [8] Eckhardt B *et al* 1995 Approach to ergodicity in quantum wave functions *Phys. Rev. E* **52** 5893–903, especially equation (24), (35), (38), (40) and (47) with  $T_H \cong 1/\hbar \cong \sqrt{\lambda} \cong R$
- [9] Fay J D 1977 Fourier coefficients of the resolvent for a Fuchsian group *J. Reine Angew. Math.* **294** 143–203, especially bottom 148–bottom 151
- [10] Hejhal D A and Rackner B N 1992 On the topography of Maass waveforms for  $PSL(2, \mathbb{Z})$  *Exper. Math.* **1** 275–305
- [11] Hejhal D A 1999 On eigenfunctions of the Laplacian for Hecke triangle groups *Emerging Applications of Number Theory* IMA vol 109 ed D Hejhal, J Friedman, M Gutzwiller and A Odlyzko (Berlin: Springer) 291–315
- [12] Hejhal D A and Strömbergsson A 2001 On quantum chaos and Maass waveforms of CM-type *Found. Phys.* **31** 519–33
- [13] Hejhal D A 1983 *The Selberg Trace Formula for  $PSL(2, \mathbb{R})$*  vol 2 (*Lecture Notes in Mathematics* vol 1001) (Berlin: Springer)
- [14] Hejhal D A 2000 On the uniform equidistribution of long closed horocycles *Asian J. Math.* **4** 839–54
- [15] Hortikar S and Srednicki N 1998 Correlations in chaotic eigenfunctions at large separation *Phys. Rev. Lett.* **80** 1646–9
- [16] Iwaniec H and Sarnak P 2000 Perspectives on the analytic theory of  $L$ -functions *GAF A 2000-Visions in Mathematics* eds N Alon, J Bourgain, A Connes, M Gromov and V Milman (Basel: Birkhauser Verlag) 705–41
- [17] Jakobson D 1994 Quantum unique ergodicity for Eisenstein series on  $PSL(2, \mathbb{Z}) \backslash PSL(2, \mathbb{R})$  *Ann. Inst. Fourier Grenoble* **44** 1477–504
- [18] Li B and Robnik M 1994 Statistical properties of high-lying chaotic eigenfunctions *J. Phys. A: Math. Gen.* **27** 5509–23
- [19] Luo W and Sarnak P 1995 Quantum ergodicity of eigenfunctions on  $PSL(2, \mathbb{Z}) \backslash H$  *Publ. IHES* **81** 207–37

- 
- [20] Magnus W, Oberhettinger F and Soni R P 1966 *Formulas and Theorems for the Special Functions of Mathematical Physics* (Berlin: Springer) pp 142 (line 11), 145 (middle)
- [21] Ozorio De Almeida A M 1988 *Hamiltonian Systems: Chaos and Quantization* (Cambridge: Cambridge University Press)
- [22] Salem R and Zygmund A 1954 Some properties of trigonometric series whose terms have random signs *Acta Math.* **91** 245–301
- [23] Sarnak P 1995 Arithmetic quantum chaos *Israel Math. Conf. Proc.* **8** 183–236
- [24] Sarnak P 1981 Asymptotic behaviour of periodic orbits of the horocycle flow and Eisenstein series *Comm. Pure Appl. Math.* **34** 719–39
- [25] Sarnak P 2001 Estimates for Rankin–Selberg  $L$ -functions and quantum unique ergodicity *J. Funct. Anal.* **184** 419–53
- [26] Srednicki M and Stiernlof F 1996 Gaussian fluctuations in chaotic eigenstates *J. Phys. A: Math. Gen.* **29** 5817–26
- [27] Voros A 1994 Aspects of semiclassical theory in the presence of classical chaos *Progr. Theor. Phys. Suppl.* **116** 17–44
- [28] Watson G N 1944 *A Treatise on the Theory of Bessel Functions* (Cambridge: Cambridge University Press)
- [29] Zelditch S 1991 Mean Lindelöf hypothesis and equidistribution of cusp forms and Eisenstein series *J. Funct. Anal.* **97** 1–49